Performance and degradation of $La_{0.8}Sr_{0.2}Ga_{0.85}Mg_{0.15}O_{3Ld}$ electrolyte-supported cells in single-chamber configuration

M. Morales [a,*], *J.M. Pérez-Falcón* [b], *A. Moure* [b], *J. Tartaj* [b], *F. Espiell* [a], *M. Segarra* [a]

[a] *Centre DIOPMA, Departament de Ciència dels Materials i Enginyeria Metal$lúrgica, Universitat de Barcelona, Martı´ i Franque`s 1, 08028 Barcelona, Spain*

[b] *Instituto de Cerámica y Vidrio (CSIC) Kelsen 5, Cantoblanco, 28049 Madrid, Spain*

Abstract

Electrolyte-supported cells were made of a La0.8Sr0.2Ga0.85Mg0.15O3—d (LSGM2015) electrolyte (200 mm thickness) prepared by ethylene glycol complex solution synthesis, isostatic pressing and sintered at 1400 ◦C, a Ni-SDC anode, a Sm0.2Ce0.8O3—d (SDC) buffer-layer be- tween anode and electrolyte, and a La0.5Sr0.5CoO3—d-SDC cathode. The cells were tested in single-chamber configuration using methaneeair mixtures. The results of X-ray diffraction and SEM-EDS showed a single-phase in the electrolyte and conductivities (w0.01 S cm—1 at 650 ◦C) close to the typical values. Good cell power densities of 215 and 102 mW cm—2 were achieved under CH4/O2 = 1.4 of at 800 and 650 ◦C, respectively. However, the cell stability tests indicated that the operating temperature strongly influenced on the cell performance after 100 h. While no significant change in the power density was observed working at 650 ◦C, a clear performance degradation was evidenced at 800 ◦C. SEM-EDS revealed an appreciable degradation of the electrolyte and both the electrodes.

1. Introduction

Last decades, great efforts have been made by many re- searchers to find new electrolyte materials in order to reduce the operating temperature of SOFCs [1,2], thus improving the chemical stability at long-term, the cost-effective materials for interconnectors and the balance of plant [3]. Sr- and Mg- doped lanthanum gallates (LaGaO3), commonly well-known as LSGM, are considered as an alternative to yttria-stabilizedzirconia (YSZ) electrolyte, especially at intermediate temper- atures (600e800 ◦C). The doping of the

LaGaO3 perovskite with Sr (in La-sites) and Mg (in Ga-sites) introduces a quantity of oxygen vacancies that results in a high conductivity (>0.10 S cm—1 at 800 ◦C) [4]. Moreover, it exhibits a negligible electronic conductivity at temperatures lower than 1000 ◦C over a broad range of oxygen partial pressures, from pureoxygen (P(O2) = 1 atm) to moistened hydrogen (P(O2) ¼ 10—22 atm), and a stable performance over long oper- ating times [4,5], resulting in a larger performance of the cell [6]. The highest oxide-ion conductivities are found for the La0.8Sr0.2Ga0.83Mg0.17O2.815 composition at 800 ◦C (0.166 S cm—1) and 700 ◦C (0.079 S cm—1), respectively [4,7]. However, LSGMceramics often present problems related to their chemical stability by the formation of resistive phases, such as LaSr- Ga3O7, LaSrGaO4 or LaGaO4 [8]. In their manufacturing pro- cess, the LSGM purity strongly depends on several factors, including the purity of starting materials, methods of powder synthesis and shaping, temperature sintering, etc. Conven- tional synthesis method by solid-state reaction (SSR) involves high sintering temperatures, which facilitate the presence of compositional inhomogeneities, due mainly to the Ga evapo- ration, thus easily leading to the formation of secondary phases [9]. Alternative synthesis routes, which are based on wet chemical synthesis, such as solegel, co-precipitation, hydrothermal synthesis, glycine-nitrate [10e13], have been proposed to reduce the final sintering temperature. The che- lation of complex cations, leading to the polyesterification in the presence of a polyhydroxy alcohol, such as ethylene gly- col, to form a polymeric resin is a cost effective and simple alternative with excellent results for both the Sr- and Mg- doped LaCrO3 and LaGaO3 ceramics [14,15]. Both the phase purity and the microstructure strongly depend on the syn- thesis method, the composition and the sintering tempera- ture, thus affecting both the electrical and mechanical properties [16].

Despite several LSGM compositions present good ionicconductivities to be used as electrolytes in SOFCs at inter- mediate temperatures [17,18], these ceramics have been not widely implemented, as these may present important chem- ical reactions with the electrodes during their sintering. The interfacial reaction between the Ni-based anode and the LSGM electrolyte has been reported in several works [19,20]. It in- duces the formation of secondary phases at the anode-and heating, increasing the (combined) efficiency even further. Thus, it is expected that these advantages could provide a fast commercialization of the SC-SOFCs during the transition phase from fossil fuels to renewable energy sources.Unfortunately, thestabilityoftheusedmaterialswithrespect to both the microstructural degradation and the material decomposition is still preventing a

broad implementation of SOFCs. As the degradation of the cells based on LSGM electrolytes is a key factor to be studied, which has been much less investigated in single-chamber configurations than in the con- ventional dual chamberdevices, the aimofthiswork isthestudyof the performance and degradation of La0.8Sr0.2Ga0.85Mg0.15O3—d(LSGM2015) electrolyte-supported cells in single-chamber configuration. We are thus continuing our investigation on single-chamber Ni-SDC/SDC/LSGM/LSC-SDC fuel cells fed by mixtures of methaneandairgas[25]. Then, the cellstability testsat short-term indicated a performance degradation around 10e15% after 55 h operating at 750 ◦C and 6 thermal cycles (be- tween theroom temperature and 750 ◦C). Now, we are extending our previous results on the cell performance degradation operating for 100 h at different temperatures, under optimal single- chamber conditions. In this case, an electrolyte with the LSGM2015 composition has been used due to its high electrical conductivity (w0.15 S cm—1 at 800 ◦C) previously reported byseveral authors [6]. After the stability tests, the microstructures of the cells have been analysed by scanning emission microscopy (SEM) and emission dispersive spectroscopy (EDS) in order to identify the causes of the performance degradation. In addi- tion, both the purity and the microstructure of the electrolytes sintered at different temperatures have been preliminary char- acterized by X-ray diffraction, SEM-EDS and impedance spectroscopy.electrolyte interface, thus causing a strong drop in the cellperformance [21]. However, it can be avoided using a buffer layer based on doped ceria between the anode and the elec- trolyte, which can suppress the migration of Ni, La and Ga [19,22]. Owing to these problems, only a few studies about LSGM cells have been reported and much less literature is available about the single-chamber SOFCs (SC-SOFCs) using LSGM as electrolyte [23e25]. SC-SOFCs operate on a uniform mixture of fuel and oxidant by ensuring the selective catalytic and electrochemical reactions on each electrode [26]. While the anode should present a higher electrocatalytic activity for the oxidation of the fuel, the cathode should exhibit a higher catalytic activity for the reduction of oxygen. So, the cell performance strongly depends on the selectivity of the electrodes and the operating conditions, such as the temperature, the flow rate and the fuel-oxidant ratio [27]. The main advantage of SC-SOFCs, with respect to the conventional dual- chamber SOFCs, is to simplify the device design and operate in mixtures of hydrocarbon (natural gas, methane, propane...) and air, without the separation between the fuel and the oxidant, as their operating temperatures are optimal for the hydrocarbon reforming in the anode, which is well-known as internal reforming [28]. Therefore, SOFCs under these condi-

tions become thermally and mechanically more resistant than conventional fuel cells. In addition, these devices generate quite heat that can be used for warm water supply

2. Experimental

2.1. Synthesis and characterization of the materials

For preparing LSGM2015 powders, stoichiometric amounts of La(NO3)3$6H2O (Merck, 99.0%), Sr(NO3)2 (Fluka, 99.0%), Ga(NO3)3$9H2O (Alfa Aesar, 99,999%), Mg(NO3)2$6H2O (Merck, 99.0%) were dissolved in nitric acid (65%) and ethylene glycol (1:8 v/v). The as-obtained solutions were thermally treated in three steps: 80 ◦C for 2 h, 120 ◦C for 3 h to obtain a black resin embedding all cations, and finally 180 ◦C up to combustion of the polymeric gel, which converted the resin into an expanded porous solid. After milling in an Agate mortar, the resulting powder was calcined at 900 ◦C for 5 h and attrition milled for 2 h in ethanol with zirconia balls. Afterwards, 1 g powder was uniaxially pressed into a pellet with 12 mm diameter at 100 MPa, isostatically pressed at 200 MPa, and finally sintered in air for 12 h at different temperatures (1400 and 1450 ◦C). After attrition milling, BET surface area of the powders was determined using a Quantachrome Accusorb instrument. The density of the sintered pellets was measured by the Archi- medes method with distilled water. The theoretical densities were calculated from the division of the molecular weight by the cell volume as proposed by Datta et al. [29], giving a value of 6.68 g cm—3 for LSGM2015. The materials were characterized by X-Ray Diffraction (XRD) in a Bruker D8 Advance diffrac- tometer (Cu Ka1 radiation) typically at 3.3$10—2 s—1 scan rate. After polishing and thermal etching, the microstructures of the sintered samples were examined by scanning electron microscopy (SEM) using a Zeiss Microscope (model DSM 950, Germany) equipped with an energy dispersive spectroscopy (EDS) detector.

Both sides of the LSGM2015 pellets sintered at different tem- peratures were dip-coated with an Ag commercial paste (Dupont) to be used as electrodes. Silver coated pellets were fired at 700 ◦C for 1 h to ensure a good adhesion between the sample surface and silver electrodes. Afterwards, the ionic conductivities were measured in a dual-chamber system, using Ceramabond 503 (Aremco, US) as sealant, under hu- midified hydrogen as fuel and oxygen as oxidant, within temperature range of 260e660 ◦C. The measurements were performed using an electrical impedance analyser (model HP-294A, Hewlett-

Packard) in the frequency range of 10 MHze100 Hz. The bulk and grain boundary conductivities were separated as presented in our previous work [30]. Due to the same experimental limitations, it was not possible to carry out measurements at temperatures higher than 660 ◦C. Three samples sintered at each temperature were analysed in order to achieve a statistical significance.

2.3. Processing and electrical performance of the electrolyte-supported cells

Six replicates of LSGM2015 electrolyte-supported cells were prepared, using the pellets sintered at 1400 ◦C, which showed the highest ionic conductivity. The experimental procedure to prepare the cells, which consisted of Ni-Sm0.2Ce0.8O3—d (SDC) as anode, SDC as buffer layer, LSGM2015 as electrolyte, and La0.5Sr0.5CoO3—d (LSC)-SDC as cathode (Fig. 1), was similar to that of our previous work [25]. A SDC buffer layer wasdeposited via screen-printing onto a side of the electrolyte in order to avoid the interfacial reactions between anode and electrolyte during the anode sintering. Then, both the LSGM2015 and SDC were co-sintered in air at 1400 ◦C for 12 h.Inks of Ni-SDC (70e30 wt.%) and LSC-SDC (80e20 wt.%), usingterpineol as solvent, were prepared as precursors of the anode and the cathode, respectively. First, the anode was deposited by screen printing on the side of the SDC buffer layer, and subsequently sintered at 1150 ◦C in 5% H2eAr for 2 h. After-wards, the cathode was screen printed on the other side of theLSGM electrolyte, and sintered at 1100 ◦C in Ar for 2 h. Thus, the cells presented 10 mm diameter, thicknesses of 200 mm for the electrolyte, 10 mm SDC buffer layer and 20e30 mm anode and cathode. The active area of the cells was 0.5 cm2. The microstructures of the cells were examined by scanning electron microscopy (SEM) using a Zeiss Microscope (model DSM 950, Germany) equipped with an energy dispersive spectroscopy (EDS) detector.

The electrical characterization of the cells was per- formed in a single-chamber configuration. In order to determine the electrical properties, platinum wires were attached to the electrode surfaces of the cells for the current collection. Inks of Ni-SDC (90e10 wt.%) and LSC-SDC-Ag2O (80e10e10 wt.%) were deposited onto the anode and the cathode, respectively, as current collectors. In addition, Ag mesh was used as an electronic collector for cathode. An additional thermocouple Pt versus Pt-10% Rh was placed in direct contact with the centre of the anode surface in order to determine the real temperature of the fuel cells. The cells were placed in a quartz tube (inner diameter of 23

mm) used as reactor, and heated by a tubular furnace at 5 ◦C min—1 under 50 ml min—1 N2 from room temperature to 850 ◦C. After that, the methane as fuel and the synthetic air (80:20% in N2 and O2, respectively) as oxidant were mixed in different CH4/O2 ratios between 0.8 and 2.0, and total flown rates from 200 to 700 ml min—1. Electromotive forces were measured using a Keithley 617 electrometer with an input resistance of 1014 U at different temperatures. The value of current was measured by recording the voltage drop in an auxiliary known resistance. The characteristic current to voltage curves (IeV) were determined by using the equip- ment for measuring current and voltage under variable loads. Finally, the stability of the cell performance with the operating time was analysed. In order to evaluate the per- formance of LSGM cells at short-time, several stability tests were performed on three cells for 100 h at different oper- ating temperatures.

3. Results and discussion

3.1. Material characterization

Fig. 2 shows the XRD patterns for the LSGM2015 composition sintered at 1400 ◦C and 1450 ◦C. A single perovskite phase (marked as "O") is only observed at the sintering temperatures of 1400 ◦C. In contrast, traces of LaSrGaO4 and LaSrGa3O7, as secondary phases, are also detected in the sample sintered at 1450 ◦C. These impurities are also identified by SEM-EDS analysis (Fig. 3). The darkest and clearest zones, marked as"1" and "2", are associated with the LaSrGa3O7 and LaSrGaO4 phases, respectively (Fig. 3(b)). So, LaSrGaO4 and LaSrGa3O7 impurities are mainly located at the grain boundaries and intragranular zones, respectively. The results and the aspect of the phases in the micrographs are in agreement with those observed by Lu et al. [21]. The distribution of impurities can be

justified by their melting points [6]. LaSrGaO4 has a low melting point, w1400 ◦C, thus probably being in liquid state at the sintering temperature (1450 ◦C) that may wet over grain boundaries. In contrast, LaSrGa3O7 presents a higher melting

point (>1600 ◦C), which does not melt at the sintering tem- perature (1450 ◦C), and thus remaining in localized points of the microstructure. On the other hand, the comparison of the

microstructure images in Fig. 3 shows that the average grain size was strongly increased with the sintering temperature from 4.1 0.4 mm (1400 ◦C) to 6.3 0.5 mm (1450 ◦C).

However, the relative density is not significantly varied, being 96.7 and 97.5% for the samples sintered at 1400 and 1450 ◦C, respec- tively. These results are comparable with the results reported by Oncel et al. [31] and Isikawa et al. [32] for single-phase LSGM2015 ceramics processed by regenerative solegel and self-propagating high temperature synthesis, respectively. Alternatively, Goodenough et al. [6,33] obtained pure pellets of
$La_{0.8}Sr_{0.2}Ga_{0.83}Mg_{0.17}O_{3-d}$ and $La_{0.8}Sr_{0.2}Ga_{0.8}Mg_{0.15}O_{3-d}$ with relative densities as high as 99%, which were obtained by solidestate reaction method and sintered at between 1430 and 1500 ◦C for 24 h.

3.2. Electrical characterization of the LSGM2015 pellets

The Arrhenius plots of the ionic conductivities for the samples sintered at different temperatures show that the highest total conductivities are achieved for the sample sintered at 1400 ◦C(Fig. 4(a)). It is attributed to that the total conductivity ismainly determined by the grain boundary conductivity (Fig. 4(b) and (c)). An increase in grain size usually reduces the grain boundary density per volume unit, thus reducing the number of grain boundaries that partially block the ionic conductivity. Therefore, the grain boundary conductivities do not significantly depend on the average grain size, because the sample with the highest grain boundary conductivity, which is sintered at 1400 ◦C, presents a smaller grain size. As sug- gested by the above mentioned XRD and SEM-EDS results, itindicates a relatively higher presence of secondary phasessegregated to the grain boundaries in the sample sintered at 1450 ◦C. These results of ionic conductivities for the LSGM2015 composition sintered at 1400 ◦C are slightly lower than thoseof LSGM1520 composition sintered at 1350 ◦C, using the samemethod based on ethylene glycol polymeric organic complex solution [15]. However, the extrapolation of the total ionic conductivities up to 800 ◦C obtained for the LSGM2015 sinteredat 1400 ◦C indicates that these would be around0.03e0.05 S cm^{-1}. As a result, these electrical properties are comparable to those of samples with different compositionsand preparation methods obtained by other authors [9e15], thus indicating that are suitable for an implementation in SOFCs.

3.3. Microstructure of the electrolyte-supported cells

Fig. 5 shows the SEM micrographs of the microstructures of the Ni-SDC/SDC/LSGM/LSC-SDC after manufacturing. The electrolyte with 200 mm thickness presented high density, and both electrodes exhibit a good porosity. It is also observed that the SDC buffer layer, which has a thickness around 10 mm, is well adhered to both LSGM electrolyte and Ni-SDC anode (Fig. 5(b)). The electrolyte-cathode interface also shows a good interfacial adhesion. In addition, the analysis of energy dispersive spectroscopy (EDS) at the anode-buffer layer-elec- trolyte and electrolyte-cathode interfaces confirm the absence of specie migration, such as Ni, La and Ga, during the sintering process.

3.4. Currentevoltage measurements of the cells

Preliminary electrical experiments revealed that the highest open circuit voltages (OCVs) and power densities of the cells were obtained at a CH4/O2 ratio of 1.4 and at 500 ml min—1 total flow rate. So, the subsequent electrical tests were performedunder these optimal conditions of both the gas composition and total flow rate. High reproducibility of the cell perfor- mances was observed after testing six identical cells for several hours. Fig. 6 shows IeV (current density and cell voltage) and IeP curves (power density derived from IeV) for a single cell using a mixture of methane as fuel and air as oxidant. IeV curves are almost straight lines, which is typical in the electrolyte-supported cells, thus indicating an almost pure ohmic control. Therefore, it allows to obtain the area specific resistance (ASR) of the cells, which represents the cell ohmic resistance by unit of area, taking the slope of the linear part of the IeV curve. ASR values of 2.2 and w0.9 U cm2 at 650 and 800 ◦C are obtained, respectively. From these ASR values the total conductivities of the cell with 200 mm electrolyte thickness could be estimated around 0.009 and 0.025 S cm—1 at 650 and 800 ◦C, respectively, thus being close to those of theLSGM2015 determined by impedance spectroscopy (w0.01 S cm—1 at 650 ◦C, and 0.03e0.05 S cm—1 at 800 ◦C that is estimated by extrapolation of conductivity values from the Arrhenius plots). So, it confirms the electrolyte ohmic resistance as the limiting factor of the overall cell performance. On the other hand, the OCVs are 0.95 and 0.88 V at 650 ◦C and800 ◦C, respectively, thus showing a good selectivity toward an electrocatalytic activity for the methane oxidation at the anode, and catalytic activity for the oxygen reduction at thecathode. In terms of maximum power densities, 102 mW cm—2at 650 ◦C and 215 mW cm—2 at 800 ◦C are achieved, respec- tively. In comparison with our recent

work [25], these perfor-mances for LSGM2015 cells are slightly lower than those of LSGM1020 ones (246 mW cm—2 at 800 ◦C), using a similar cell design (SDC buffer layer and electrodes) and also under sition). It can be related to the ionic conductivity, which is critical in an electrolyte-supported cell, thus being for the LSGM2015 composition lower than LSGM1020 one. In contrast, OCV values in methane are close to those of LSGM1020 cells, because this electrical parameter mainly depends on the electrodes, buffer layer, electrolyte thickness and operating conditions, which are similar in both studied compositions. The performances obtained in the present work are compa-rable to those of Hibino et al. [23,24], which reportedmaximum power densities around 350 and 450 mW cm—2 foran electrolyte-supported SC-SOFC using LSGM1020 as an electrolyte (0.18 mm thickness) and methane as fuel at 700 and 800 ◦C, respectively. In contrast, Fukui et al. [34] reportedpower densities as high as 0.7 W cm—2 at 800 ◦C and0.4 W cm—2 at 700 ◦C in a cell with a LSGM1020 electrolytethickness of 130 mm, operating with 97% H2 and 3% H2O as fuel, and air as oxidant. So, it can be attributed to that they oper- ated in dual-chamber configuration with a highly concen-trated fuel in H2.optimal operating conditions (temperature and feed compo3.5. Cell stability tests

The stability and the degradation of the electrolyte-supported cells have been investigated for 100 h at cell temperatures of 650 and 800 ◦C and under optimal operating conditions: a CH4/ O2 ratio of 1.4 and a total flow rate of 500 ml min—1. The results of the OCVs and the power densities as a function of the operating time are presented in Fig. 7. Initially, both electrical parameters of the cells at both temperatures are slightly increased, which can be attributed to the conditioning of the electrodes and the electrode-electrolyte interfaces. After- wards, the cell performance operatingat 650 ◦C remains almost constant with the time. In contrast, the OCV is slightly reduced and the power density is decreased at 800 ◦C. Therefore, the performance stability of these cells significantly depends on the operating temperature. In order to better analyse the effect of cell degradation, polarization curves have been determined before and after the test. As shown in Fig. 8, the cell perfor- mance is nearly unchanged after 100 h operating at 650 ◦C.However, a clear degradation of the performance is observed after 100 h working at 800 ◦C, as the IeV slopes before and afterthe stability tests are different. The ASR of the cells operated at 800 ◦C increases from w0.9 U cm2 (after 4 h) to w1.2 U cm2 after
100 h of stability test. So, this decrease of the performance may be attributed to the

degradation of the electrolyte and both the electrodes, as evidenced in Fig. 9. Some delaminations at the Ni-SDC/SDC interface (Fig. 9(b)), which could be due to local redox cycles and thermal oscillations during the operation time. Almost no carbon deposit is detected by SEM-EDS anal- ysis, suggesting that the carbon deposition is limited during cell operation, and it cannot contribute to the performance degradation. In addition, a coarsening of Ni particles at theanode is also observed after the stability test at 800 ◦C (Fig. 9(d)).

The cathode microstructure also shows a slight coarsening (Fig. 9(e)e(g)). Some zones of LSGM electrolyte at the LSC-SDC/ LSGM interface present secondary phases, which are observed by SEM-EDS analysis and marked as "1" in Fig. 9(e), thus also contributing to the decrease of the cell performance. In contrast, the Ni-SDC/SDC/LSGM interface does not present significant changes by chemical reactivity. Finally, the use of a silver mesh embedded between cathode layer/ink and the metallic silver present in the current collector could be also

degraded operating at 800 ◦C, as it melts at temperatures around 960 ◦C.4.

Conclusions

LSGM2015 electrolyte-supported cells in single-chamber configuration, using methaneeair mixtures, have achieved good power densities at 800 ◦C (215 mW cm—2) and 650 ◦C (102 mW cm—2) under a CH4/O2 ratio ¼ 1.4. The cell electrolyte,which has been synthesized by ethylene glycol complex solu- tion and sintered at 1400 ◦C, shows no presence of secondary phases, and conductivities (around 0.01 S cm—1 at 650 ◦C) similar to the typical values of LSGM materials. The stabilitytests have indicated that the cell performance remains almost constant operating at 650 ◦C for 100 h. In contrast, the OCV slightly decreases and the power density is significantly degraded at 800 ◦C, thus increasing the cell ASR from w0.9 U cm2 to w1.2 U cm2. This decrease of the performance isattributed to the degradation of both electrodes, such as the coarsening of the Ni and LSC particles at the anode and cath- ode, and the delamination of the Ni-SDC/SDC interface. In addition, the formation of secondary phases at the LSC-SDC/ LSGM interface also contributes to the performance degrada- tion. However, almost no carbon deposit is detected by SEM- EDS analysis, suggesting that the carbon deposition is limited during cell operation. In conclusion, these results demonstrate that the operating

temperature within range of 650e800 ◦Ccritically influences on the degradation of the performance and microstructure of a LSGM2015 electrolyte-supported SC-SOFC.

Acknowledgements

This work was partially funded by the Spanish Government MAT2011-23623 and XaRMAE (Xarxa de Refere`ncia en Mate- rials Avanc¸ ats per l'Enginyeria, Generalitat de Catalunya).

R E F E R E N C E S

[1] Hoogers G. Fuel cell technology handbook. Boca Raton, FL: CRC Press; 2003.

[2] US Department of Energy. Fuel cell handbook. 7th ed. Office of Fossil Energy, National Energy Technology Laboratory; 2004.

[3] Steele BC. Ceramic ion conducting membranes. Solid State Mater Sci 1996;1:684e91.

[4] Ishihara T, Matsuda H, Takita Y. Doped LaGaO3 perovskite type oxide as a new oxide ionic conductor. J Am Chem Soc 1994;116:3801e3.

[5] Huang PN, Petric A. Superior oxygen ion conductivity of lanthanum gallate doped with strontium and magnesium. J Electrochem Soc 1996;143:1644e8.

[6] Huang KQ, Tichy RS, Goodenough JB. Superior perovskite oxide-ion conductor; strontium- and magnesium-doped LaGaO3: I, phase relationships and electrical properties. J Am Ceram Soc 1998;81:2565e75.

[7] Djurado E, Labeau M. Second phases in doped lanthanum gallate perovskites. J Eur Ceram Soc 1998;18:1397e404.

[8] Li S, Bergman B. Doping effect on secondary phases, microstructure and electrical conductivities of LaGaO3 based perovskites. J Eur Ceram Soc 2009;29:1139e46.

[9] Kuncewicz-Kupczyk W, Kobertz D, Miller M, Singheiser L, Hilpert K. Vaporization of Sr- and Mg-doped lanthanum gallate and implications for solid oxide fuel cells. J Electrochem Soc 2001;148:E276e81.

[10] Cho YH, Ha SB, Jung DS, Kang YC, Lee JH. SiO2-Tolerant grain-boundary

conduction in Sr- and Mg-doped lanthanum gallate. Electrochem Solid St 2010;13:B28e31.

[11] Pelosato R, Cristiani C, Dotelli G, Latorrata S, Ruffo R, Zampori L. Coprecipitation in aqueous medium of La0.8Sr0.2Ga0.8Mg0.2O3—d via inorganic precursors. J Power Sources 2010;195:8116e23.

[12] Chen T-Y, Fung KZ. Synthesis and densification of oxygen- conducting La0.8Sr0.2Ga0.8Mg0.2O2.8 nano powder prepared from a low temperature hydrothermal urea precipitation process. J Eur Ceram Soc 2008;28:803e10.

[13] Li Z-C, Zhang H, Bergman B, Zou X. Synthesis and characterization of La0.85Sr0.15Ga0.85Mg0.15O3—delectrolyte by steric entrapment synthesis method. J Eur Ceram Soc 2006;26:2357e64.

[14] Duran P, Tartaj J, Capel F, Moure C. Formation, sintering and thermal expansion behaviour of Sr- and Mg-doped LaCrO3 as SOFC interconnector prepared by the ethylene glycol polymerized complex solution synthesis method. J Eur Ceram Soc 2004;24:2619e29.

[15] Morales M, Roa JJ, Pe´rez-Falco´ n JM, Moure A, Tartaj J, Segarra M. Electrical and mechanical characterization by instrumented indentation technique of La0.85Sr0.15Ga0.8Mg0.2O3—d electrolyte for SOFCs. J Eur Ceram Soc 2012;32:4287e93.

[16] Morales M, Roa JJ, Perez-Falco´ n JM, Moure A, Tartaj J, Espiell F, et al. Correlation between electrical and mechanical properties in La1—xSrxGa1—yMgyO3—d ceramics used as electrolytes for solid oxide fuel cells. J Power Sources 2014;246:918e25.

[17] Wan JH, Yan JQ, Goodenough JB. LSGM-based solid oxide fuel cell with 1.4 W/cm2 power density and 30 day long-term stability. J Electrochem Soc 2005;152:A1511e5.

[18] Lee D, Han JH, Kim EG, Song RH, Shin DR. Characterization of co-doped LSGM electrolyte prepared by GNP for IT-SOFC. J Power Sources 2008;185:207e11.

[19] Zhang X, Ohara S, Maric R, Okawa H, Fukui T, Yoshida H,
et al. Interface reactions in the NiO-SDC-LSGM system. Solid State Ionics 2000;133:153e60.

[20] Kim KN, Kim BK, Son JW, Kim J, Lee HW, Lee JH, et al. Characterization of the electrode and electrolyte interfaces of LSGM-based SOFCs. Solid State Ionics 2006;177:2155e8.

[21] Lu XC, Zhu JH. Effect of Sr and Mg doping on the property and performance of the La1—xSrxGa1—yMgyO3—d electrolyte. J Electrochem Soc 2008;155:B494e503.

[22] Huang K, Wan JH, Goodenough JB. Increasing power density of LSGM-based solid oxide fuel cells using new anode materials. J Electrochem Soc 2001;148:A788e94.

[23] Hibino T, Hashimoto A, Inoue T, Tokuno J, Yoshida S,
Sano M. A low-operating temperature solid oxide fuel cell in hydrocarbon-air mixtures. Science 2000;288:2031e3.

[24] Hibino T, Hashimoto A, Inoue T, Tokuno J, Yoshida S,
Sano M. A solid oxide fuel cell using an exothermic reaction as the heat source. J Electrochem Soc 2001;148:A544e9.

[25] Morales M, Roa JJ, Tartaj J, Segarra M. Performance and short- term stability of single-chamber solid oxide fuel cells based on La0.9Sr0.1Ga0.8Mg0.2O3—d electrolyte. J Power Sources
2012;216:417e24.

[26] Yano M, Tomita A, Sano M, Hibino T. Recent advances in single-chamber solid oxide fuel cells: a review. Solid State Ionics 2007;177:3351e9.

[27] Morales M, Pinˇ ol S, Segarra M. Intermediate temperature single-chamber methane fed SOFC based on Gd doped ceria electrolyte and La0.5Sr0.5CoO3—d as cathode. J Power Sources 2009;194:961e6.

[28] Shao ZP, Mederos J, Chueh WC, Haile SM. High power- density single-chamber fuel cells operated on methane. J Power Sources 2006;162:589e96.

[29] Datta P, Majewski P, Aldinger F. Synthesis and microstructural characterization of Sr- and Mg-substituted LaGaO3 solid electrolyte. J Alloys Compd 2007;438:232e7.

[30] Moure A, Castro A, Tartaj J, Moure C. Single-phase ceramics with La1—xSrxGa1—yMgyO3—d composition from precursors obtained by mechanosynthesis. J Power Sources
2009;188:489e97.

[31] Oncel C, Ozkaya B, Gulgun MA. X-ray single phase LSGM at 1350◦C. J Eur Ceram Soc 2007;27:599e606.

[32] Ishikawa H, Enoki M, Ishihara T, Akiyama T. Self- propagating high-temperature

synthesis of La(Sr)Ga(Mg)O3—d for electrolyte of solid oxide fuel cells. J Alloys Compd 2007;430:246e51.

[33] Huang K, Wan J, Goodenough JB. Oxide-ion conducting ceramics for solid oxide fuel cells. J Mater Sci 2001;36:1093e8.

[34] Fukui T, Ohara S, Murata K, Yoshida S, Miura K, Inagaki T. Performance of cells with La(Sr)Ga(Mg)O3 electrolyte film. J Power Sources 2002;106:142e5

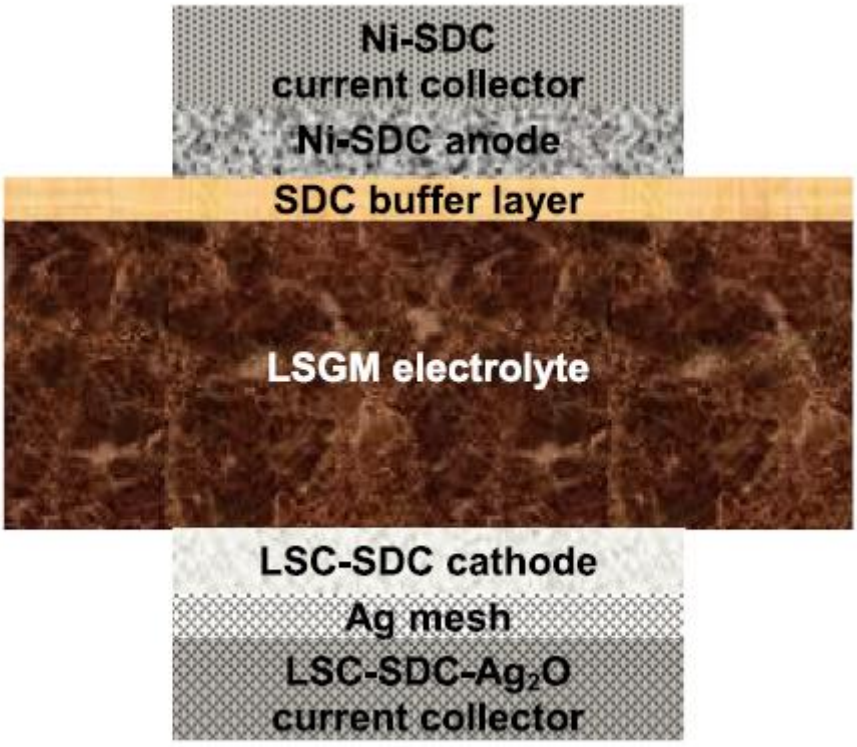

Figure 1. Schematic configuration of the LSGM2015 electrolyte supported cells

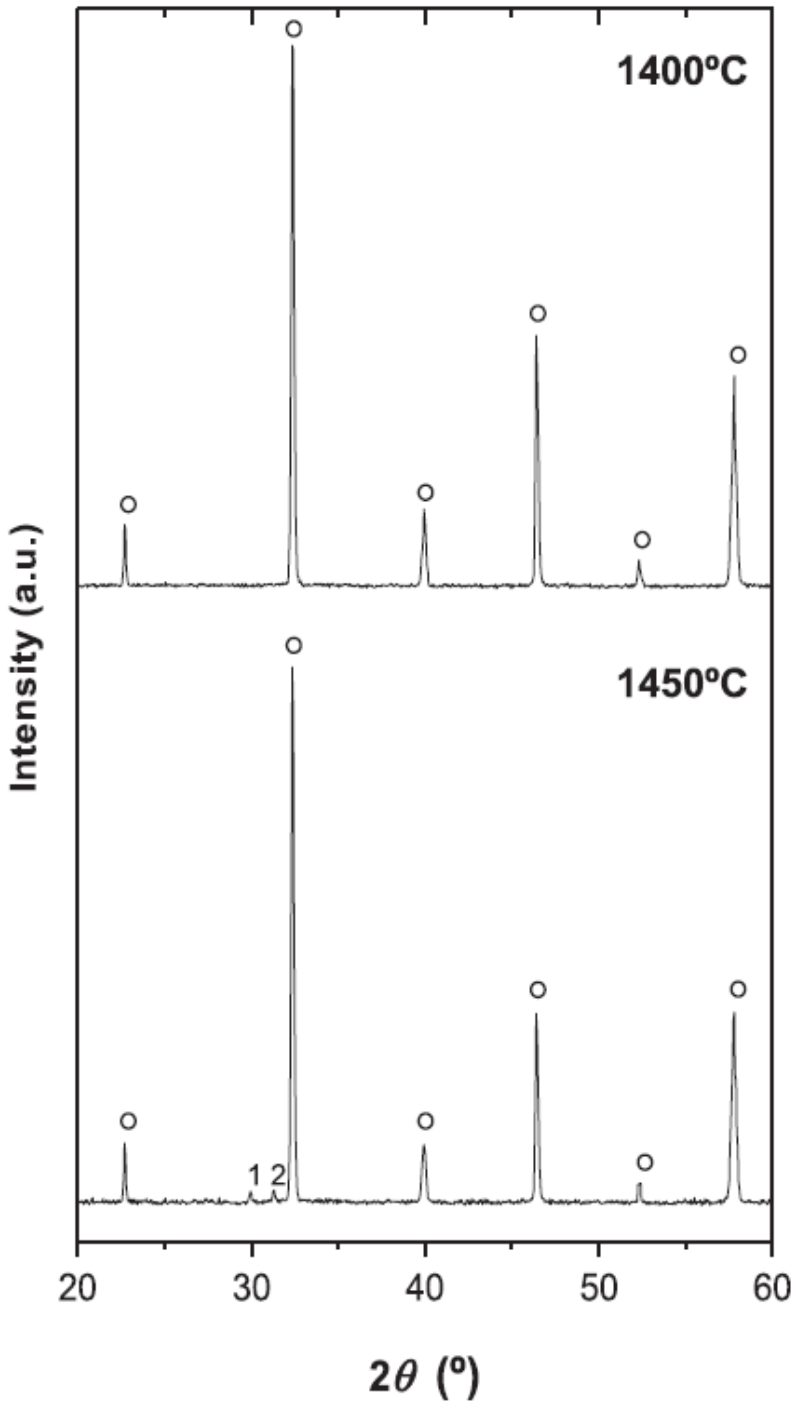

Figure 2. XRD patterns of the LSGM 2015 pellets at different sintering temperatures for 12h in the range 20-60º (o, LSGM perovskite; 1 LaSrGaO7; 2 LaSrGaO4

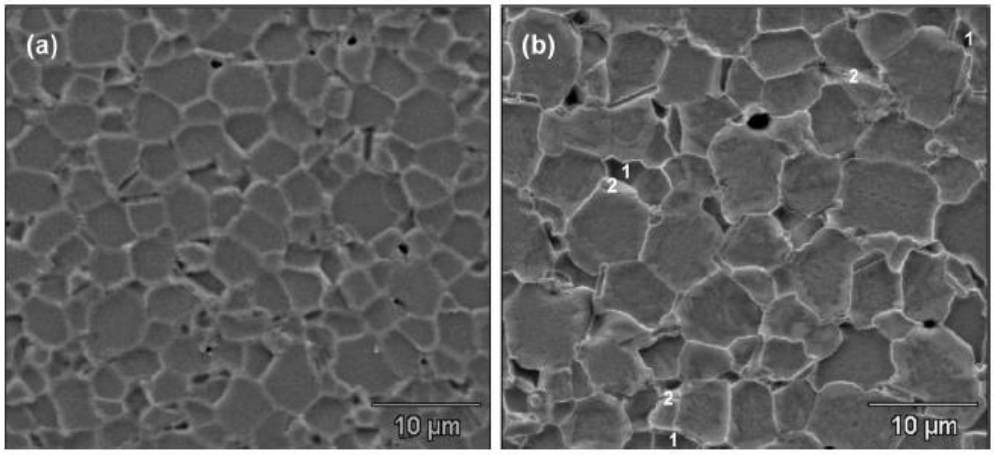

Figure 3. SEM micrographs of LSGM2015 sintered at a) 1450ºC for 12 h (1 LaSrGaO7; 2 LaSrGaO4)

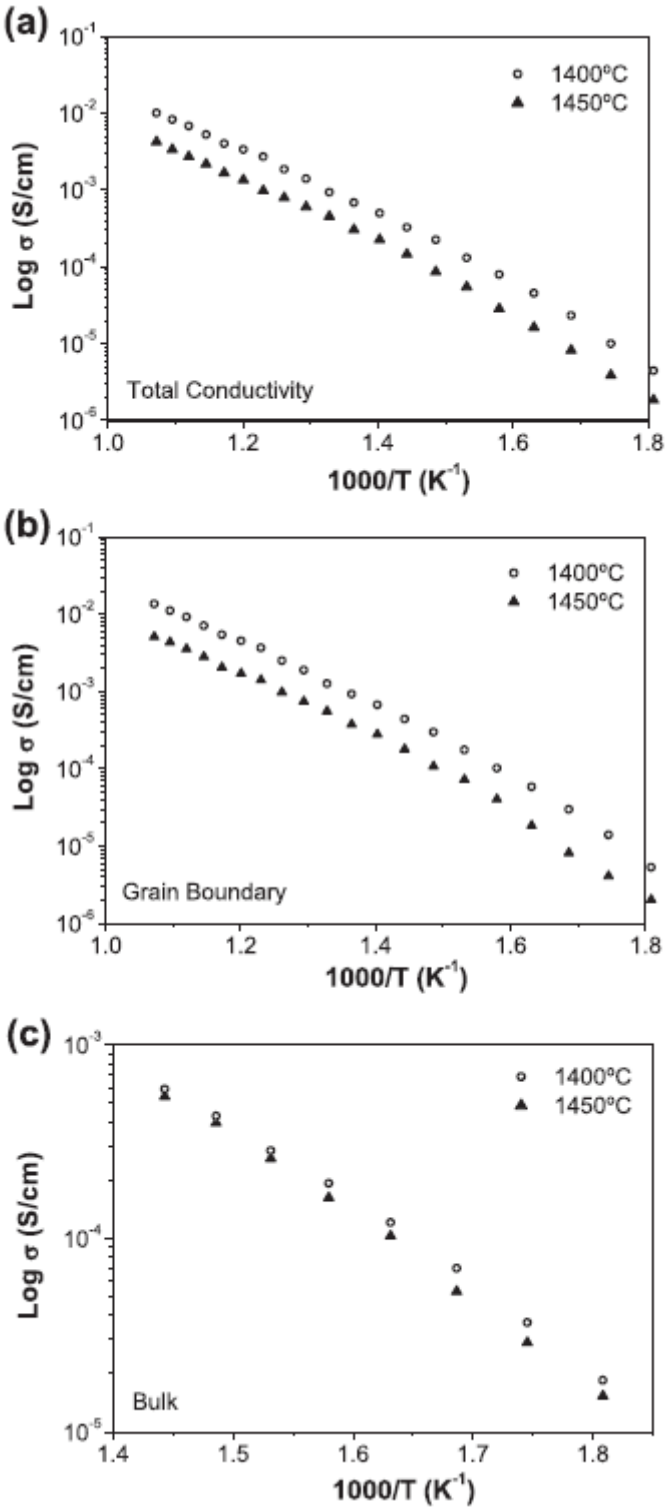

Figure 4. Fig. 4 e Arrhenius plots of: (a) the total, (b) the grain boundary, and (c) the bulk conductivity of LSGM2015 ceramics sintered at different temperatures

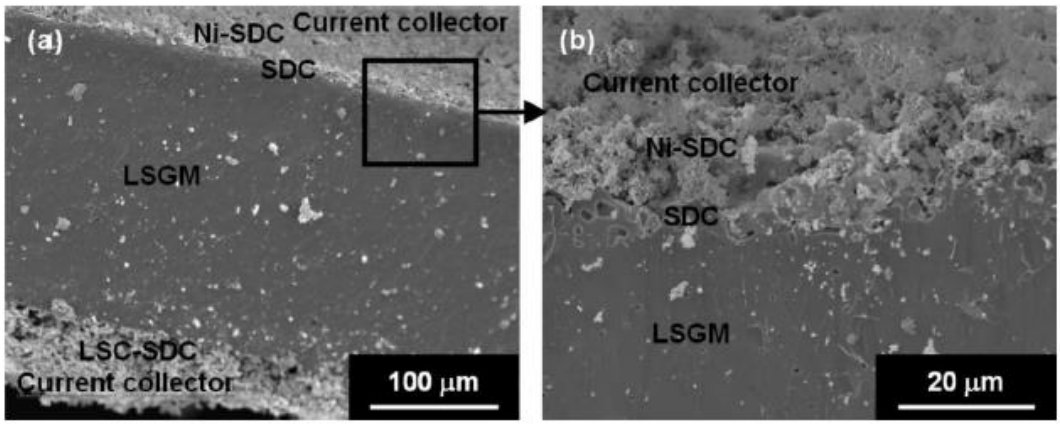

Fig. 5 SEM micrographs of the cross-sectional of: (a) the LSGM2015 electrolyte-supported cell, and (b) the anode-buffer layer-electrolyte interface

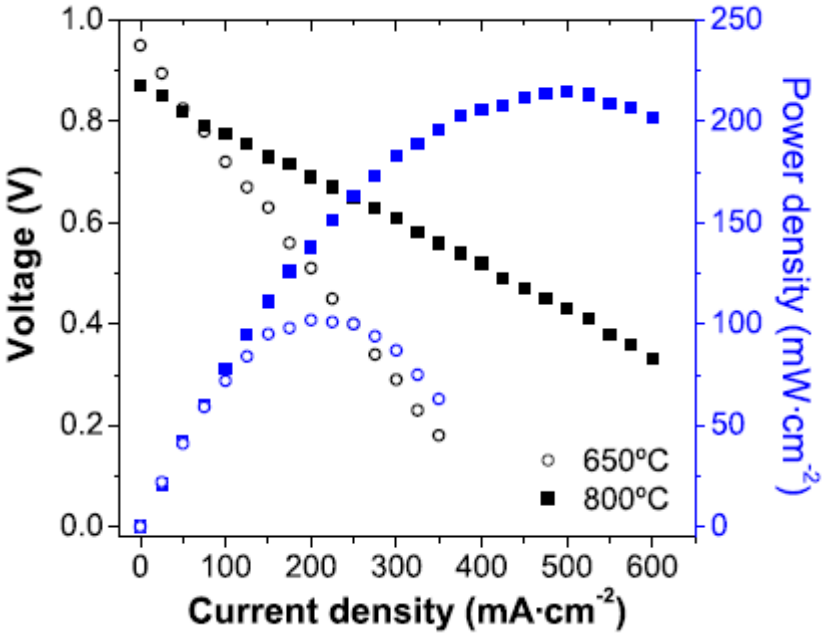

Figure 6. Cell performance measured at 650ºC and 800ºC, a CH4/O2 ratio of 1.4 and a total flow rate of 500 ml/min

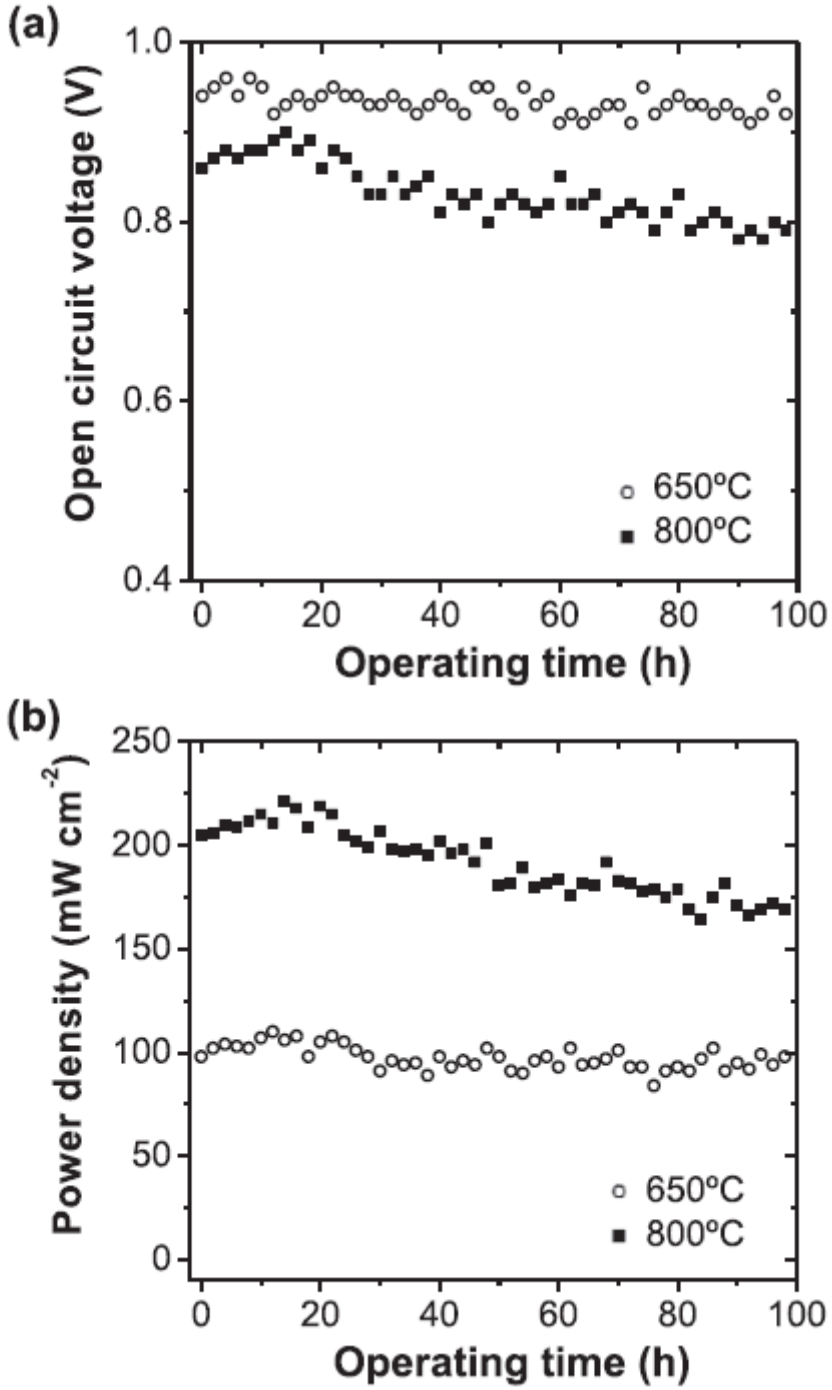

Fig. 7 (a) Cell open circuit voltage, and (b) power density (at 0.45 V) with the operating time at 650 and 800 ◦C, a CH4/ O2 ratio of 1.4 and a total flow rate of 500 ml minL1

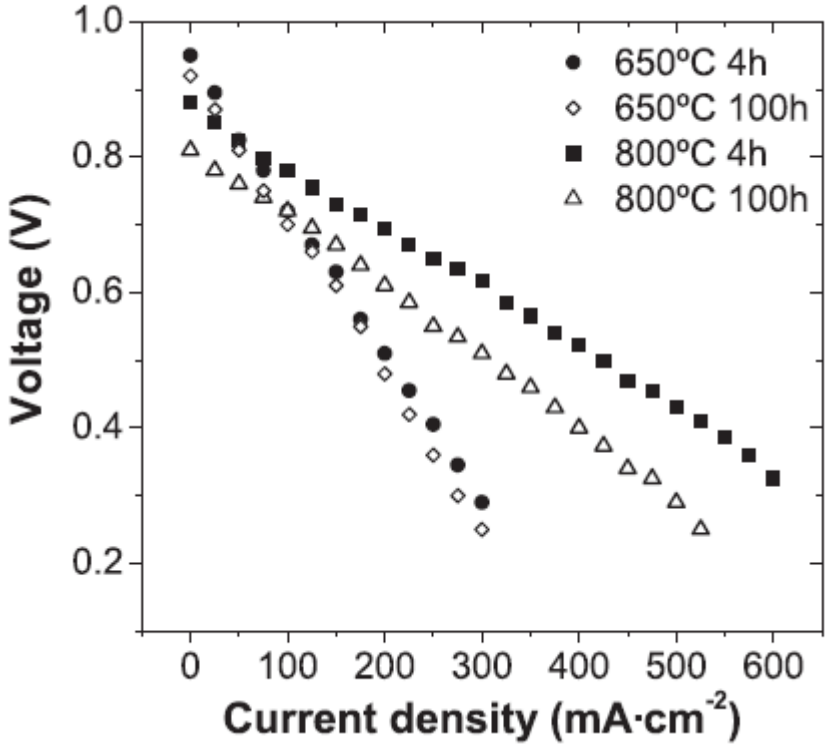

Fig. 8 IeV curves after 4 h and 100 h operating at 650 and 800 ◦C, a CH4/O2 ratio of 1.4 and a total flow rate of 500 ml minL1

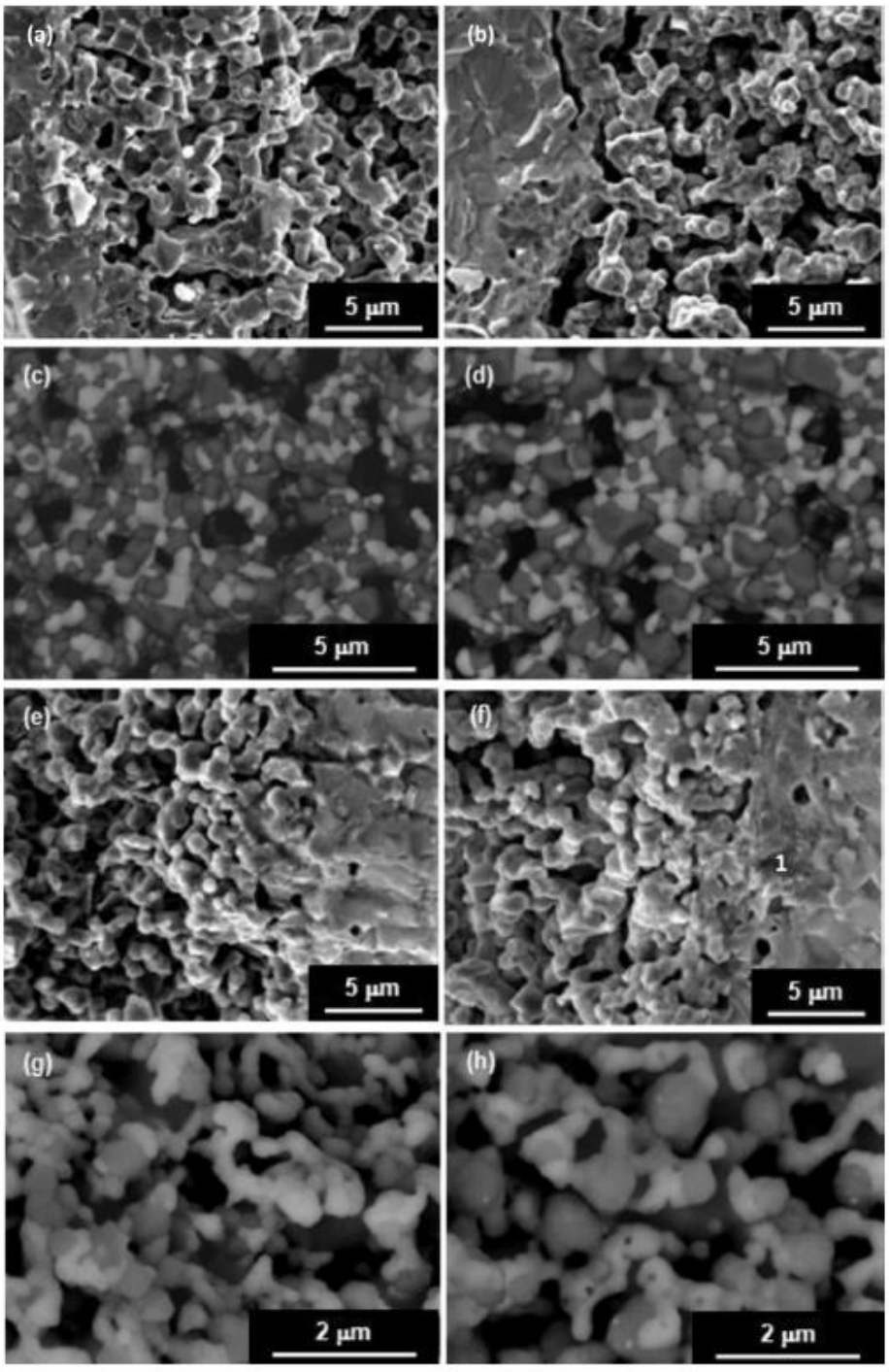

Fig. 9 SEM micrographs of: (a) and (b) Ni-SDC/SDC/LSGM interface before and after testing at 800 ◦C for 100 h, (c) and (d) Ni- SDC anode before and after testing, (e) and (f) LSC-SDC/LSGM interface before and after testing, (g) and (h) LSC-SDC cathode before and after testing